Evolution of the large scale circulation, cloud structure and regional water cycle associated with the South China Sea monsoon during May-June, 1998

K.-M. Lau[1] and Xiaofan Li[2]

Laboratory for Atmospheres, NASA/Goddard Space Flight Center, Greenbelt, MD

June, 2001

(Submitted to J. Meteor. Soc. Japan)

[1] Dr. William K.-M. Lau, Climate and Radiation Branch, Laboratory for Atmospheres, NASA/GSFC, Greenbelt, MD 20771. Email: lau@climate.gsfc.nasa.gov

[2] NOAA/NESDIS, Camp Springs, Washington DC.

Abstract

In this paper, changes in the large-scale circulation, cloud structures and regional water cycle associated with the evolution of the South China Sea (SCS) monsoon in May-June 1998 were investigated using data from the Tropical Rainfall Measuring Mission (TRMM) and field data from the South China Sea Monsoon Experiment (SCSMEX). Results showed that both tropical and extratropical processes strongly influenced the onset and evolution of the SCS monsoon. Prior to the onset of the SCS monsoon, enhanced convective activities associated with the Madden and Julian Oscillation were detected over the Indian Ocean, and the SCS was under the influence of the West Pacific Anticyclone (WPA) with prevailing low level easterlies and suppressed convection. Establishment of low-level westerlies across Indo-China, following the development of a Bay of Bengal depression played an important role in building up convective available potential energy over the SCS. The onset of SCS monsoon appeared to be triggered by the equatorward penetration of extratropical frontal system, which was established over the coastal region of southern China and Taiwan in early May. Convective activities over the SCS were found to vary inversely with those over the Yangtze River Valley (YRV).

Analysis of TRMM microwave and precipitation radar data revealed that during the onset phase, convection over the northern SCS consisted of squall-type rain cell embedded in meso-scale complexes similar to extratropical systems. The radar Z-factor intensity indicated that SCS clouds possessed a bimodal distribution, with a pronounced signal (>30dBz) at a height of 2-3 km, and another one (>25 dBz) at the 8-10 km level, separated by a well-defined melting level indicated by a bright band at around 5-km level. The stratiform-to-convective cloud ratio was approximately 1:1 in the pre-onset phase, but

increased to 5:1 in the active phase. Regional water budget calculations indicated that during the active phase, the SCS was a strong sink ($E-P<<0$) of atmospheric moisture, with the primary source of moisture coming from regions further west over Indo-China and the eastern Indian Ocean. Before onset and during the break, the SCS was a moisture source ($E-P>0$) to the overlying atmosphere. In particular, the SCS provided the bulk of moisture to the torrential rain over the YRV in mid-June 1998.

1. Introduction

The South China Sea (SCS) is an important region where the Asian monsoon commences each year around mid-May (Tao and Chen 1987, Lau and Yang 1997, Lau et al. 1998, Hsu and Chen 1999). Climatologically, the onset of rainfall and the development of southwesterly wind occur in late April or early May in northern SCS, followed by a wind shift in the lower troposphere from easterly to westerly in the southern SCS (Lau et al. 1998, Ding et al. 1999, Li and Qu 1999). Convective activities in the vicinity of northern SCS and the Philippines have been related to interannual and intraseasonal rainfall variability over mainland China and Japan, as well as summertime teleconnection signals over the North Pacific (Nitta 1987, Huang and Sun 1992, Lau and Peng 1992, Chen et al. 2000, Lau and Weng 2000a, b).

Because of the importance of the SCS monsoon in affecting the summertime climate and regional water cycle over Southeast and East Asia, the South China Sea Monsoon Experiment (SCSMEX) was conducted in May-June 1998. The purpose of SCSMEX was to study monsoon processes and their roles in the maintenance of the hydrologic cycle of the East and Southeast Asian monsoon region, with the aim towards improving monsoon rainfall prediction. Observational platforms in SCSMEX included enhanced soundings from stations and ships, dual Doppler Doppler radars, aerosondes, surface flux measurements from ships and buoys, and satellite-derived ocean surface wind and rain products from TRMM and scatterometer. Details of the observational platforms, data description, and preliminary results have been reported in Lau et al. (1999). In this paper, we focused on the changes of the large-scale monsoon circulation, rainfall, cloud structure, and regional water cycle associated with the evolution of the SCS monsoon.

2. Data

For the analysis of the large scale circulation, and regional water calculations, we used analyzed wind and moisture data from the SCSMEX soundings (Johnson and Ceisleski 1999). The wind data has horizontal and vertical resolutions of 2°x2° and 25mb respectively. Scatterometer wind at 10 m derived from SSM/I data (Atlas et al. 1996) was used to extend the SCSMEX domain to include the Indian Ocean and the western Pacific. For rainfall and convective intensity, we used rainfall data from the Tropical Rainfall Measuring Mission (TRMM). The TRMM satellite has provided the surface rain rate and vertical profile of hydrometeors over the entire tropics between 40°S and 40°N since November 1997 (Kummerow et al. 2000, Oki et al. 1998). TRMM data used in this study included: i) daily mean rain rate (2A12) constructed from TRMM Microwave Imager (TMI) surface rain rate with the horizontal resolution of 0.5°x0.5°, ii) reflectivity (2A25) from the TRMM precipitation radar (PR), with vertical resolution of 250 m and horizontal resolution of 5-km, and iii) fractional covers of stratiform and convective clouds (2A23) from PR derived from 2A25.

3. SCS monsoon onset and large scale evolution

The evolution of the SCS summer monsoon during May- June 1998 is well captured by the surface observations (Fig. 1, courtesy of Prof. P. L. Liam) at Dongsha Island, which is located at 117°E, 21°N in the northern SCS. The surface wind at the site fluctuated from northeasterly to southwesterly during the entire month of May due to development of a quasi-stationary front over the region (Chang and Chen 1995). The monsoon onset was signaled by sudden shifts in fluctuation regimes in relative humidity,

surface pressure and surface temperature. Before May 16, pronounced diurnal cycles were observed. After May 16, as the monsoon conditions developed, the diurnal cycles were diminished, accompanied by rising relative humidity, falling surface pressure and temperature. The rain gauges at Dongsha also recorded generally enhanced rainfall during the active monsoon period (May 16 – June 8). Sporadic heavy rain episodes found in early and mid-May can be attributed to influence from the aforementioned frontal systems. The active monsoon conditions abruptly ended around June 8, after which the diurnal cycles resumed, and the surface wind turn steady southerlies during June 12- 21, signaling a break in the SCS monsoon. As shown later, the monsoon break coincided with the advance of the monsoon trough to the East Asian continent and the development of the *Mei-yu* rain band over the Yangtze River Valley (YRV) which began around the second week in June 1998.

Figures 2 and 3 show the time evolution of the large-scale surface wind derived from SSM/I and rain rate from TRMM Goddard Profiling algorithm (GPROF) during the period encompassing the onset of the SCS monsoon and the occurrence of heavy rainfall over the YRV. During the early part of May (Fig. 2a), the West Pacific Anticyclone (WPA) dominated the large-scale circulation pattern over the subtropical western Pacific from equator to 35° N. Clear sky and strong easterly winds prevailed over the western tropical Pacific and the SCS on May 14 and thereabout. A quasi-stationary, pre-monsoon front system was developed and anchored over southeastern China and Taiwan at the northwestern rim of the WPA (Fig.2b). At this time, convection was notably intense over the Indian Ocean, where a large-scale anticylconic gyre circulation was emerging. The intense convection over the Indian Ocean could be traced back to convection that occurred

over the coast of eastern Africa about a week earlier (not shown). The convective complex can be identified with the supercloud cluster associated with the Madden and Julian Oscillation (MJO) (Nakazawa 1987, Lau et al. 1988). The MJO signature was evident in a pair of cyclones straddling the equator on both hemispheres, which were especially pronounced on May 14 (Fig. 2b). Shortly afterwards, the frontal system intensified and began to move eastward and southeastward while the WPA retreated eastward.

The eastward shift of the WPA was accompanied by the strengthening of equatorial westerlies over the Indian Ocean, as the MJO intensified and propagated eastward. On May 18 (Fig.2c), the MJO double cyclone bifurcated away from the equator in both hemispheres. The southern cyclone eventually dissipated while the northern cyclone propagated northeastward and developed into a major monsoon depression over the Bay of Bengal around May 18-20. The vertical wind profile over the central SCS (not shown here, see Fig. 4 in Lau et al. 1999) indicated that the entire tropospheric wind system developed a strong easterly shear (low level westerly and upper level easterlies) around May 18-20, signaling the onset of the SCS monsoon. During the , prevailing low level westerly and southwesterly winds developed over the large pat of the SCS, as the frontal system swept southeastward into the tropical western Pacific (Fig. 2d). Frequent outbreak of deep convection occurred over the SCS west of the Philippines during the active phase of the SCS monsoon from May 20 – June 8 (Fig. 2e, f). The sequence of events were remarkably similar to that observed in May 1997 (Lau et al. 1998).

At the end of the active period around June 5 - 9, the frontal rain band was re-established over northern SCS, with pronounced southerly flow over the SCS (Fig.3a). At this time, the India monsoon was ready to erupt, as indicated by the onset of heavy rain near the west coast of the Indian subcontinent, and the establishment of the Indian Ocean gyre circulation. By June 9 (Fig.3b), the WPA had fully retreated eastward, and a monsoon depression was re-developed over the Bay of Bengal. Strong low-level southerlies over the SCS continued to transport moisture from the SCS into southern China throughout the break period. The strong and steady southerly flow pushed the monsoon trough poleward, leading to the establishment of the *Mei-yu* front and torrential rainfall over the YRV beginning June 13 (Fig. 3c). From June 17-21 the monsoon rain band vascillated between the YRV and southern China causing widespread flooding in the region, while the SCS region remained quiescent during that period (Fig. 3d and e). After June 21, the SCS monsoon was revived, as indicated by the re-appearance of deep convection over SCS (Fig. 3f).

4. Composite Analysis

Fig. 4 shows the time series of TMI surface rain rate averaged over the SCS (10-24°N, 108-122°E) and the YRV (24-38°N, 116-130°E) respectively. Rainfall over the two areas were nearly out of phases. The mean rain rate over the SCS began to increase significantly around May 15, and reached the first peak of 15 mm day^{-1} on May 16-17. The rain rate experienced several peaks of approximately 24 mm day^{-1} before it reached its minimum on June 12. For the purpose of quantifying the intensity and structural changes in convection and for the computation of the regional water budget, we defined four different phases of the evolution of the large scale SCS monsoon as: pre-onset (May 9-14),

onset (May 15-19), active phase (May 20-June 11), and break phase (June 12-21). The dates are chosen based on major shifts in the large-scale circulation.

a. Kinematics

Figure 5 shows the horizontal distributions of time-mean TMI surface rain rates, winds and divergences at 200 and 850mb based on the SCSMEX wind analysis, for the four phases of the SCS summer monsoon respectively. The area mean values of the key dynamical quantities over the SCS region referred to in the following discussion can be found in Table 1. The pre-onset phase was characterized by suppressed convection (Fig. 5a, upper panel) and widespread subsidence over the SCS, as indicated by the negative divergence at 200mb and positive divergence at 850mb. The WPA was fully extended westward, prevailing over the entire SCS and the Indo-China region. Moderate northwesterly wind at 200mb and the southeasterly winds at 850mb were found over the SCS. Over the land mass of East Asia, active mid-latitude disturbances were evident in a pronounced 200mb jetstream, strong 200mb divergence (middle panel), and 850mb convergences and cyclonic activities (lower panel). While rainfall is light, with area mean of 1 mm/day, the convective available potential energy, (CAPE ~1.69×10^3 Jkg^{-1}) over the SCS during the pre-onset was the highest among the four phases, implying that this was also a build-up phase for the SCS monsoon.

During the onset phase (Fig.5b), deep convection as indicated by heavy rain cells developed along a southwest-northeast swath from the Bay of Bengal, across Indo-China to the East China Sea (upper panel). The area mean rain rate increased to 11 mm/day. The convection over northern SCS was associated with equatorial penetration of an extratropical front coming from central East Asia, as evident in the southward shift of the

200mb jetstream, and the development of pronounced low level southwesterly flow over southern China and Taiwan. The complex of heavy rain cells over the Bay of Bengal was associated with the development of a strong monsoon depression as indicated by the 200mb anticyclone (middle panel) and the 850mb cyclone (lower panel) over the region. The sequence of events suggests that the the low level southwesterly wind over Indo-China, spawned by the Bay of Bengal depression may have been instrumental in transporting moisture into the SCS through. Over the SCS, positive divergence at 200mb ($\sim 0.17 \times 10^{-5}$ s^{-1}) coupled with convergence at 850mb ($\sim -0.09 \times 10^{-5}$ s^{-1}) implied upward motion, and a favorable environment for initiation of deep convection. The flaring up of convection over the SCS, mostly triggered by squall-type frontal systems led to partial release of CAPE ($\sim 138 \times 10^{3}$ Jkg^{-1}), amount to 20% reduction of CAPE from its pre-onset or build-up phase.

During the active phase, deep convection became more frequent over the SCS, with heavy rain cells anchored to the west of the Philippines (Fig.5c, upper panel). The upper level anticyclone over Indo-China was fully developed with the westerly jet was found at the southernmost position near 20°N (middle panel). Concomitantly the WPA was fully retracted eastward, and low level westerly wind with averaged speed of ~ 4-5 ms^{-1} blew from the eastern Indian Ocean across Indo-China to the SCS (lower panel). The divergence at upper troposphere and the convergence at the lower troposphere peaked during this period (see Table 1). Rainfall over the SCS was heaviest (~27 mm/day), and the CAPE was at its lowest ($\sim 1.18 \times 10^{3}$ Jkg^{-1}), approximately a 30% reduction from the onset phase. This energy was presumably released into kinetic energy in driving the SCS monsoon. During the break phase, deep convection mostly vanished over the SCS, and a

zonally oriented frontal system established over the YRV near 30°N (Fig. 5c, upper panel). The mean rain rate dropped to approximately 3 mm/day. At this stage, the upper level westerly jet was re-established at 35- 40°N and a pronounced anticyclone developed downstream of the Tibetan Plateau (middle panel). Over SCS, the upper level convergence (~0.19×10^{-5} s^{-1}) at 200mb and low-level divergence (~0.06×10^{-5} s^{-1}) at 850mb indicated the resumption of large scale subsidence, and a re-build up of CAPE (~ 1.61×10^{3} Jm^{-2}) over the region. Strong southerly wind (~5.1 m/s) over the SCS and southwesterly wind from Burma and southwestern China converged into the *Mei-yu* front over the YRV.

b. Cloud structure

Changes in cloud structure, and rain systems associated with the four stages of the SCS monsoon will be discussed in this section. To illustrate the cloud structure associated with the SCS convection. Figure 6 shows a snapshot of TMI surface rain rate, PR reflectivity (corrected Z factor) at 2.5-km level, and vertical cross section of PR Z factor along 16.5°N and 17°N on May 20, 1998. Associated with the southward penetration of the frontal rain band, multiple heavy rain cells developed, which were oriented in the southwest-northeast direction (Fig. 6, upper left). Embedded with the heavy rain cell, the PR data indicated a meso-scale complex with squall-line structure including deep convective cores at the leading edge, with trailing stratiform clouds (Fig. 6, upper right). The size of the deep convective cores in the leading edge (represented by contours of the Z factor higher than 40 dBz) was not larger than 20x20 km^2. The trailing stratiform region (>30 dBz) spanned an area of approximately 50 km to 100 km.

The vertical structure (Fig.6, lower panel) provided a snapshot of complex convective processes within the mesoscale system. As indicated by coincident ground

radar echo (Tom Keenan, private communication), the convective complex was moving southwestward at the time of the snapshot. At the leading (western) portion of the system, a developing convective chimney and a dying convective element was detected. The leading convective chimneys (>40dBz) reached to about 5 km, and upper level stratiform cirrus anvil (>20dBz) developed up to 10 km in the vicinity of the convective core. In between the leading cell and the main cell, is a region of reduced reflectivity, where downdraft was likely to be prevalent. The main cell possessed a spatial scale of about 100 km, within which strong convective activity (>40dBz) appeared to be maintained over a large horizontal fetch at the 5 km level, which coincides with the melting level for tropical convection. This suggested that the main cell was in its mature development being maintained by microphysical and mesoscale processes in the middle and upper troposphere. Further separated from the main cell was a trailing convective cell, probably near the end of its life cycle.

Because of the lack of spatial and temporal sampling of the PR data, individual convective events cannot be followed. Here, we used a composite method to delineate the possible changes in convective and cloud structures associated with different stages of the SCS monsoon. Figure 7 shows the probability distribution functions for the PR data as a function of height and PR values, also known as Contoured Frequency Altitude Diagram (CFAD, Yuter and Houze 1995). Here contour values represent the percentage of occurrences for a given range of PR values and altitude that fell with the spatial and temporal domain for the SCS monsoon stages. The fractional covers for convective and stratiform rain (2A23) were compiled for different SCS monsoon phases and shown in Table 2a.

During the pre-onset phase (Fig.7a), only weak signals were detected below the melting level (~5 km). Water clouds associated with shallow convection covered about 1-2 % of the total SCS area with maxima at 2-km level. In all, there were about equal amount of stratiform vs. convective rain (Table 1). During the monsoon onset phase (Fig.7b), the CFAD assumed a distinct bimodal distribution centered around 30 dBz and altitude of 2-4 km, and 20 dBz at 6-10 km, with a clear separation at approximately 5.5 km. The first mode was associated with deep convective cores, generally associated with larger drop size and water clouds covering 4% of total area, while the second mode indicated developing stratiform anvils and ice clouds above the melting level with approximately 6 % coverage. In the onset phase, the TRMM data indicated a stratiform-to-convective cloud (S/C) ratio of 3.2 (Table 2a). In the mature phase (Fig.7c), the CFAD was basically similar to the onset phase, showing an increased frequency of occurrence of both convective and stratiform cloud types. Interestingly, the stratiform cloud showed more substantial increase, with the 20dBz signal reaching above 10 km. At the active phase, the bright band at the melting level at 5.5 km was also well-defined indicating the active conversion process within vigorous convective systems. As shown in Table 2, the stratiform clouds increased to 11%, while the convective clouds increased to 2.1%, yielding a S/C ratio of 5.1. The above results suggested that the active phase was characterized by more mature convective cells with large anvil clouds over the SCS region. During the break (Fig.7d), the CFAD was similar to the pre-onset phase, with mostly low-level water clouds. Some weak signals were found above the melting level, probably due to remnants of deep convection from the mature phase, and conditions more

favorable for generation of upper level clouds in an already moist environment compared to the pre-onset phase.

As a comparison, the CFAD for the *Mei-yu* cloud systems over the YRV region (25 N – 35°N, 116-128°E) before and during the development of the torrential rain was shown in Fig. 8. The former was within the active phase, and the latter coincided with the break phase of the SCS monsoon. The structure changes of the *Mei-yu* cloud systems shown in Fig. 8a and b indicated a near reversal of those between the mature and the break phases of the SCS monsoon (Fig. 7c and d). While the anvil cloud distribution during YRV heavy rain was similar to the active SCS cloud system, the signal below the melting level was lesser pronounced compared with the SCS clouds. The difference suggested that mid-latitude processes, i.e., stratiform clouds associated with frontal development may be more important for sustaining the *Mei-yu* system during 1998. On the other hand, stronger development of convective cells might be favored or required to support the convective complex in the tropical environment of the SCS. Overall, the S/C ratio for the *Mei-yu* system was generally larger than the SCS system (Table 2a). Before the YRV flooding, deep convection was scarce (0.16%), while stratiform clouds had a moderate coverage of 2.4%, giving a large S/C ratio of 15.2. The development of deep convection in the *Mei-yu* system during the YRV flood yielded a C/S ratio of about 7, more comparable to that for the mature phase of the SCS system.

c. Regional water budget

The total columnar water budgets were computed over the SCS area (8 –24°N, 108 –122°E) and the YRV region (24 – 36°N, 116 –130°E). The total moisture tendency

(TMT), the net moisture convergence (NMC), precipitation (P), and surface evaporation (E) are governed by the following water vapor conservation equation:

$$\frac{\partial < q >}{\partial t} + \nabla \bullet < qV >= E - P \tag{1}$$

wherer < > denotes vertical integral from the earth surface to the top of the atmosphere. The first and second terms on the left hand side of (1) denote the total moisture tendency (TMT) and the net moisture convergence (NMC) respectively. Summing over the entire domain, (1) becomes:

$$\text{TMT} = \text{NMC} - \text{P} + \text{E}$$

$$\text{NMC} = F_S - F_N + F_W - F_E \tag{2}$$

where F_N, F_S, F_W and F_E represents the mean contribution to the net moisture convergence by fluxes across the north, south, east and west boundaries of the domain respectively. TMT and NMC were computed by using the SCSMEX sounding data, and E-P computed as the residual. The estimated values of all the terms in (2) for different phases of the SCS monsoon were shown in Fable 3a. TMT was found to be very small compared to all the other terms. During the pre-onset phase, NMC was negative, consistent with the prevailing low-level divergence over the SCS. The SCS region received moisture (=1.4 units, with one unit equal to 10^{13} kg/day) from the eastern boundary, as a result of prevailing surface easterlies from the WPA, while transporting a large portion (=3.1 units) to the land region to the north. There was a net moisture divergence out of the region, and the SCS served as a net moisture source to the overlying atmosphere (E-P > 0). In contrast, during onset phase, the SCS region gained moisture mostly from the western boundary (= 2.1 unit), losing about half of it (=1.0 unit) to the land region to the north.

Here, the total moisture was building up at a rate of 0.4 units, and the net water balance (E-P~ 0) indicated a nearly local recycling of water within the SCS. In the active phase, all the transport into the SCS appeared to be derived from the western boundary (=5.3 units), with a substantial fraction (=2.1 units) coming out of the eastern boundary into the western Pacific. During the active phase, the budget numbers indicated about 60% of the precipitation was derived from the east-west transport, and 40% from the surface evaporation over the SCS. During the break phase, the NMC over the region became negative, with the region continued to gain moisture (= 3.0 uits) from the west. Here the north-south transport became as important as the east-west transport consistent with the change of the SCS monsoon circulation regime, and the shift of rainfall into the YRV region (see Fig. 4). A similar water budget over the YRV (Table 3b) showed that before onset, E-P was relatively small (=0.3 units), indicating local water recycling. However, during the *Mei-yu* development, the YRV region was a large moisture sink, with a large portion of its moisture convergence coming from the northward water flux from the SCS.

5. Conclusion

We carried out a study of the evolution in the 3-D large-scale circulation, rain, cloud structure and components of the water cycle with respect to the different phases the SCS monsoon. The sequence of events suggested that the SCS summer monsoon onset was triggered in part by the southward invasion of the mid-latitude frontal system concomitant with the eastward retreat of the western Pacific Subtropical High. The SCS monsoon onset was preconditioned by the moisture transport associated with development of the Bay of Bengal depression and surface westerlies over Indo-China. The Bay of Bengal depression was developed from a bifurcation of a double cyclone couplet and was

presaged by the propagation of MJO from the western equatorial Indian Ocean into the southern Bay of Bengal. The actual trigger of the SCS monsoon during 1998 appeared to be associated with the southward penetration of an extratropical front into the SCS. We also found an apparent inverse relationship between rainfall variation over the SCS and the YRV.

The structural changes in convection were identified during different phases of the SCS monsoon. Before onset, shallow water clouds dominated over the SCS with a C/S ratio about 1:1. During onset and active phase, the vertical distribution of rain activities as detected by PR showed a bimodal distribution, delineating the presence stratiform rain associated ice clouds, and convective rain in water clouds. Mature SCS convection possessed a stratiform-to-convective ratio of approximately 5:1. The vertical structure and proportion of convective and stratiform clouds further showed similarity to extratropical convective systems, and confirmed the importance of extratropical influences on convection over northern SCS.

Water budget calculations showed that during the pre-onset phase, the SCS was a moisture source, with large positive E-P. During the onset, most of the water was nearly recycled within the SCS. The situation changed drastically during the active phase, when the SCS became a strong moisture sink ($E-P<<0$), and was dominated by transport of moisture from regions further west, over Indo-China and the eastern Indian Ocean. At the break phase, northward moisture transport out of the SCS became important, and the SCS served as a moisture source for the development of *Mei-yu* rain band, and the torrential rain over the YRV in June 1998.

Acknowledgment This research is supported by the TRMM Project of NASA Earth Science Enterprise. Most of the work was carried out while the second author Dr. X. Li as an employee of Emergent Information Technologies, Inc. Vienna, Virginia. Dr. H. T. Wu provided the plots of the SSM/I wind and Prof. P. L. Liam provided the Dongsha Island data.

Table Captions

Table 1 Areal mean dynamical characteristics over the SCS during different stages of the SCS monsoon as defined in the text.

Table 2a. Fractional covers of stratiform clouds (S) and convective clouds (C) and ratio of Fs to Fc over the SCS area.

Table 2b. As Table 2a except over the Yangtze River area.

Table 3a Estimate of the various terms in the water budget (in units of 10^{13} Kg/day) over the SCS region

Table 3b. As in Table 2a, except for water budget over the YRV region

Table 1 Areal mean dynamical characteristics over the SCS during different stages of the SCS monsoon as defined in the text.

	200 mb Div (10^{-5} s^{-1})	500 mb Div (10^{-5} s^{-1})	850mb u (m/s)	850mb v (m/s)	Precipitation (mm/day)	CAPE (10^3J/kg)
Pre-onset	-0.61	0.17	-2.0	2.86	1.12	1.69
Onset	0.17	-0.09	0.20	2.78	11.09	1.38
Active	0.22	-0.16	4.0	2.39	25.88	1.18
Break	-0.19	0.06	3.5	5.1	2.99	1.61

Table 2a. Fractional covers of stratiform clouds (S) and convective clouds (C) and ratio of Fs to Fc over the SCS area.

Days	S	C	S/C
10-14 May	0.5	0.5	1.1
15-19 May	5.9	1.9	3.2
25-29 May	10.9	2.2	5.1
14-18 June	1.4	0.8	1.8

Table 2b. As Table 2a except over the Yangtze River area.

Days	S	C	S/C
20-24 May	2.4	0.2	15.2
14-18 June	6.2	0.9	6.9

Table 3a Water budget (10^{13} Kg/day) over the SCS region

	TMT	NMC	F_N	F_S	F_W	F_E	E - P
Pre-onset (5/9-5/14)	0.3	-1.6	3.1	-0.1	0.2	-1.4	1.9
Onset (5/15-5/19)	0.4	1.1	1.0	0.5	2.1	0.5	-0.7
Active (5/25-5/29)	0.2	3.2	0.6	0.6	5.3	2.1	-3.0
Break (6/14-6/18)	0.1	-0.7	4.3	1.9	3.0	1.4	0.8

Table 3b. As in Table 2a, except for water budget over the YRV region

	TMT	NMC	F_N	F_S	F_W	F_E	E - P
Pre-YRV (5/20-5/24)	0.3	0.0	0.9	-1.0	-1	-0.9	0.3
YRV (6/14-6/18)	0.0	3.8	0.2	4.1	5.4	5.5	-3.8

References

Atlas, R., R. N. Hoffman, S. C. Bloom, J. C. Jusem, and J. Ardizzone, 1996: A multiyear global surface wind velocity dataset using SSM/I wind observations. *Bull. Amer. Meteor. Soc.*, **77**, 869-882.

Chang, C.-P., and G. T. Chen, 1995: Tropical circulations associated with southwest monsoon onset and westerly surges over the South China Sea. *Mon. Wea. Rev.* **123**, 3254-3267.

Chen, T. C., M. C. Yen and S.-P. Weng, 2000: Interaction between the summer monsoons of East Asia and the South China Sea: Intraseasonal Monsoon modes. *J. Atmos. Sci.*, **57**, 1373-1392.

Ding, Yihui and collaborators, 1999: Onset and activities of Asian monsoon and heavy flooding in China in 1998. In . *Onset and evolution of the South China Sea monsoon and its interaction with the ocean.* Eds. Y. Ding and C. Li, 193-199.

Hsu, H. H., and C. T. Chen, 1997: Evolution of large scale circulation and heating during the first transition of the Asian summer monsoon. *J. Climate.*, **12**, 793-810.

Huang, R.-H., and F. Y. Sun, 1992: Impacts of the tropical western Pacific on the East Asian summer monsoon. *J. Meteor. Soc. Japan*, **70**, 243-256.

Johnson, R., P. Ciesielski, J. Knievel and M. D. Parker, 1999: Preliminary results from the South China Sea Monsoon Experiment Sounding Network. *Preprints, 23rd Conference on Hurricanes and Tropical Meteorology, Amer. Met. Soc.*, 11-14 , January 1999. Dallas, TX, 969-972.

Kummerow, C. and collaborators: 2000: The status of the Tropical Rainfall Measuring Mission (TRMM) after two years in orbit, *J. Appl. Meteor.*, **39**, 1965-1982.

Lau, K. M. and H. Weng, 2000a: Remote forcing of US summertime droughts and floods by the Asian monsoon? *GEWEX News*, **10**, May Issue, 5-6.

Lau, K. M. and H. Weng, 2000b: Teleconnection linking summertime rainfall variability over North America and East Asia. *CLIVAR Exchanges*, **5**, 18-20.

Lau, K. M. , T. Nakazawa, and C. H. Sui, 1991: Observations of cloud cluster hierarchies over the tropical western Pacific. *J. Geophys. Res., Sp. Supplement*, **96**, 3197-3208.

Lau, K.. M., Y. Ding, J. T. Wang, R. Johnson, T. Keenan, R. Cifelli, J. Gerlach, O. Thiel, T. Rickenbach, S. C. Tsay, and P. Lin, 1999: A report of the field operations and early results of the South China Sea Monsoon Experiment (SCSMEX). *Bull. Am. Meteor. Soc.* , 81, 1261-1270.

Lau, K.-M. and L. Peng, 1992: Dynamics of atmospheric teleconnection during the northern summer. *J. Climate.*, **5**, 140-158.

Lau, K.-M., and S. Yang, 1997: Climatology and Interannual variability of the Southeast Asian summer monsoon. *Adv. Atmos. Sci.*, **14**, 141-162.

Lau, K.-M., H. T. Wu and S. Yang, 1998: Hydrologic processes associated with the first transition of the Asian summer monsoon: a pilot satellite study. *Bull. Am. Meteor. Soc.*, **79**, 1871-1882.

Li, Chongyin and Qu Xin, 1999: Characteristics of atmospheric circulation associated with summer monsoon onset in the South China Sea. In *Onset and evolution of the South China Sea monsoon and its interaction with the ocean.* Eds. Y. Ding and C. Li, 200-209.

Nakazawa , T., 1988: Tropical super clusters within intraseasonal variations over the western Pacific. *J. Meteor. Soc. Japan*, **66**, 823-839.

Nitta, T., 1987: Convective activities in the tropical western Pacific and their impact on the northern hemisphere summer circulation. *J. Meteor. Soc. Japan*, **41**, 373-390.

Oki R, Furukawa K, Shimizu S, Suzuki Y, Satoh S, Hanado H, Okamoto K, Nakamura K, 1998: Preliminary results of TRMM: Part I, a comparison of PR with ground observations, *Mar. Technol. Soc. J.* **32**, 13-23.

Tao, S. and L. Chen, 1987: A review of recent research in the East Asian summer monsoon in China. in *Monsoon Meteorology*, Eds. C.-P. Chang and T. N. Krishnamurti, Oxford Univeristy Press, pp 60-92.

Yuter, S. E., Houze R. A., 1995: 3-Dimensional kinematic and microphysical evolution of Florida cumulonimbus. 2. Frequency distributions of vertical velocity, reflectivity, and differential reflectivity. *Mon. Wea. Rev.*, **123**, 1941-1963.

Figure Captions

Fig. 1 Time series of surface wind vector (m/s), relative humidity (%), surface pressure (mb), surface temperature (^{o}C), and rainfall (mm) observed at Dongsha Island during May-June 1998 (Courtesy of Prof. P. L. Liam, National Central University).

Fig. 2 Daily-mean surface rain rate from TRMM GPROF and surface wind from SSM/I for May- 10 –30, 1998.

Fig. 3. Same as Fig. 2, except for June 5-25.

Fig. 4 Time series of TMI daily surface rain rates (mm/day) averaged over the SCS (solid line) and over the Yangtze River area (dashed line).

Fig. 5 Horizontal distributions of pentad mean TMI surface rain rates (upper panel), streamline and divergence (10^{-6} s^{-1}) at 200 mb (middle panel) and at 850 mb (lower panel). The pentads are chosen to represent a) he pre-onset phase , b) the onset phase, c) active phase and d) the break phase.

Fig. 6 Horizontal distribution of TMI derived surface rain rate (upper left panel) and PR corrected Z factor at 2.5-km level (upper right panel), and vertical cross section of corrected Z factor along 16.5^{o}N (lower panel) on 20 May 1998.

Fig. 7 Vertical distributions of probability distribution functions of PR Corrected Z factor over the SCS area during (a) pre-onset, (b) onset, (c) active, and (d) break of the SCS monsoon

Fig. 8 As in Fig 10 except over the Yangtze River area for (a) pre-heavy rain and (b) during heavy rain periods.

June 1998.

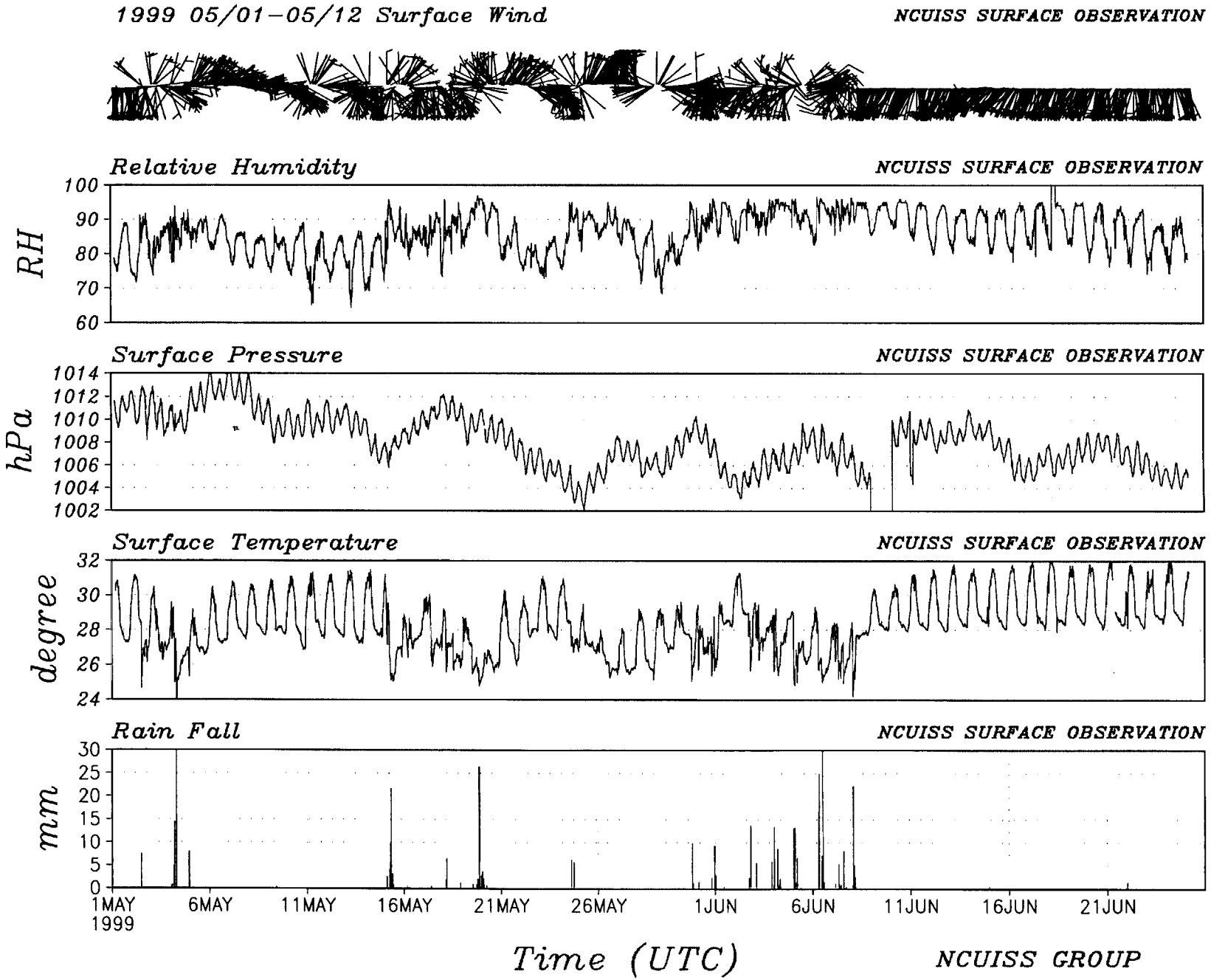
1999 05/01-05/12 Surface Wind
NCUISS SURFACE OBSERVATION
Relative Humidity
NCUISS SURFACE OBSERVATION
RH
100
90
80
70
60
Surface Pressure
NCUISS SURFACE OBSERVATION
hPa
1014
1012
1010
1008
1006
1004
1002
Surface Temperature
NCUISS SURFACE OBSERVATION
degree
32
30
28
26
24
Rain Fall
NCUISS SURFACE OBSERVATION
mm
30
25
20
15
10
5
0
1MAY
1999
6MAY
11MAY
16MAY
21MAY
26MAY
1JUN
6JUN
11JUN
16JUN
21JUN
Time (UTC)
NCUISS GROUP

Figure 1

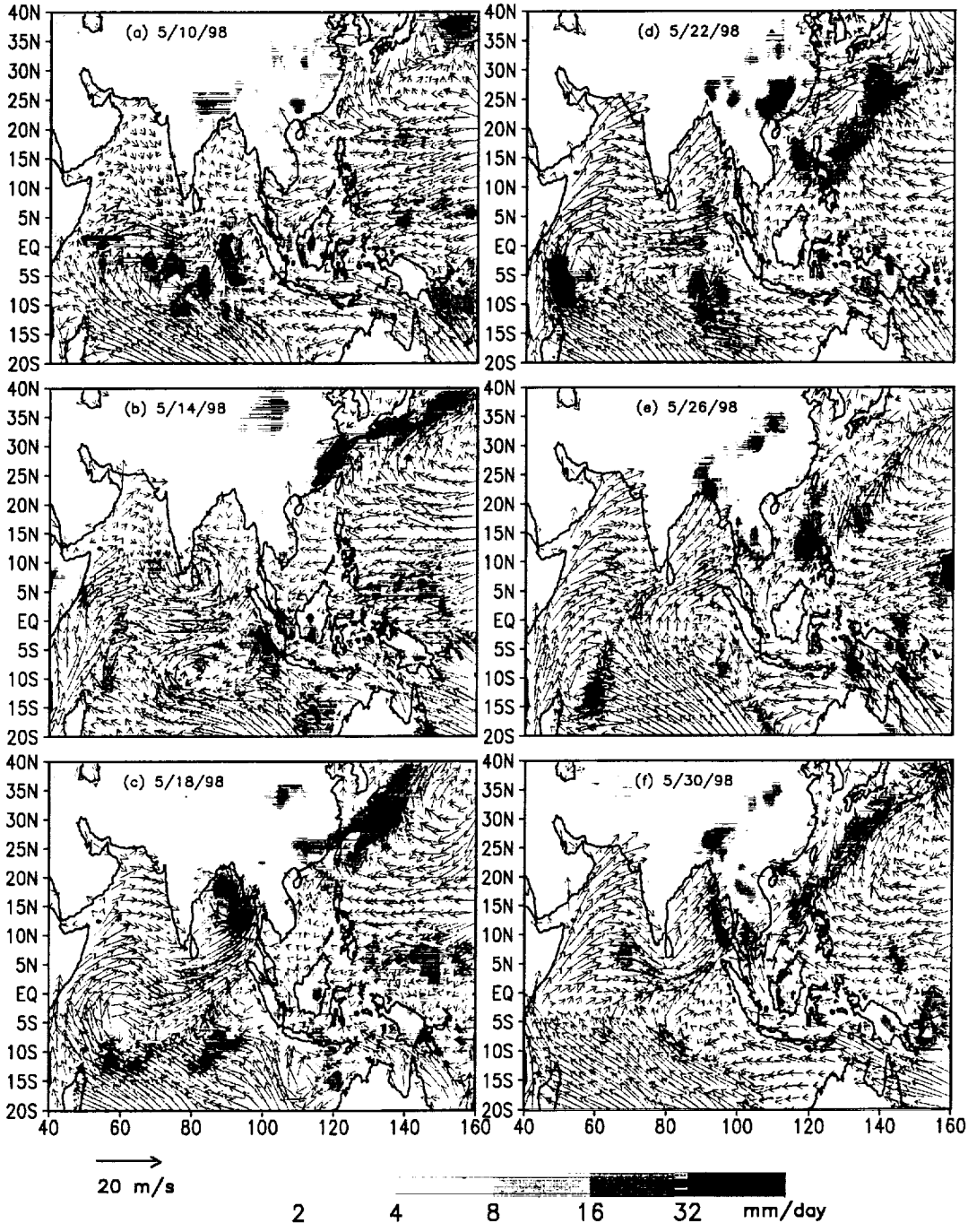
(a) 5/10/98
(b) 5/14/98
(c) 5/18/98
(d) 5/22/98
(e) 5/26/98
(f) 5/30/98
40N
35N
30N
25N
20N
15N
10N
5N
EQ
5S
10S
15S
20S
40
60
80
100
120
140
160
20 m/s
2
4
8
16
32
mm/day

Figure 2

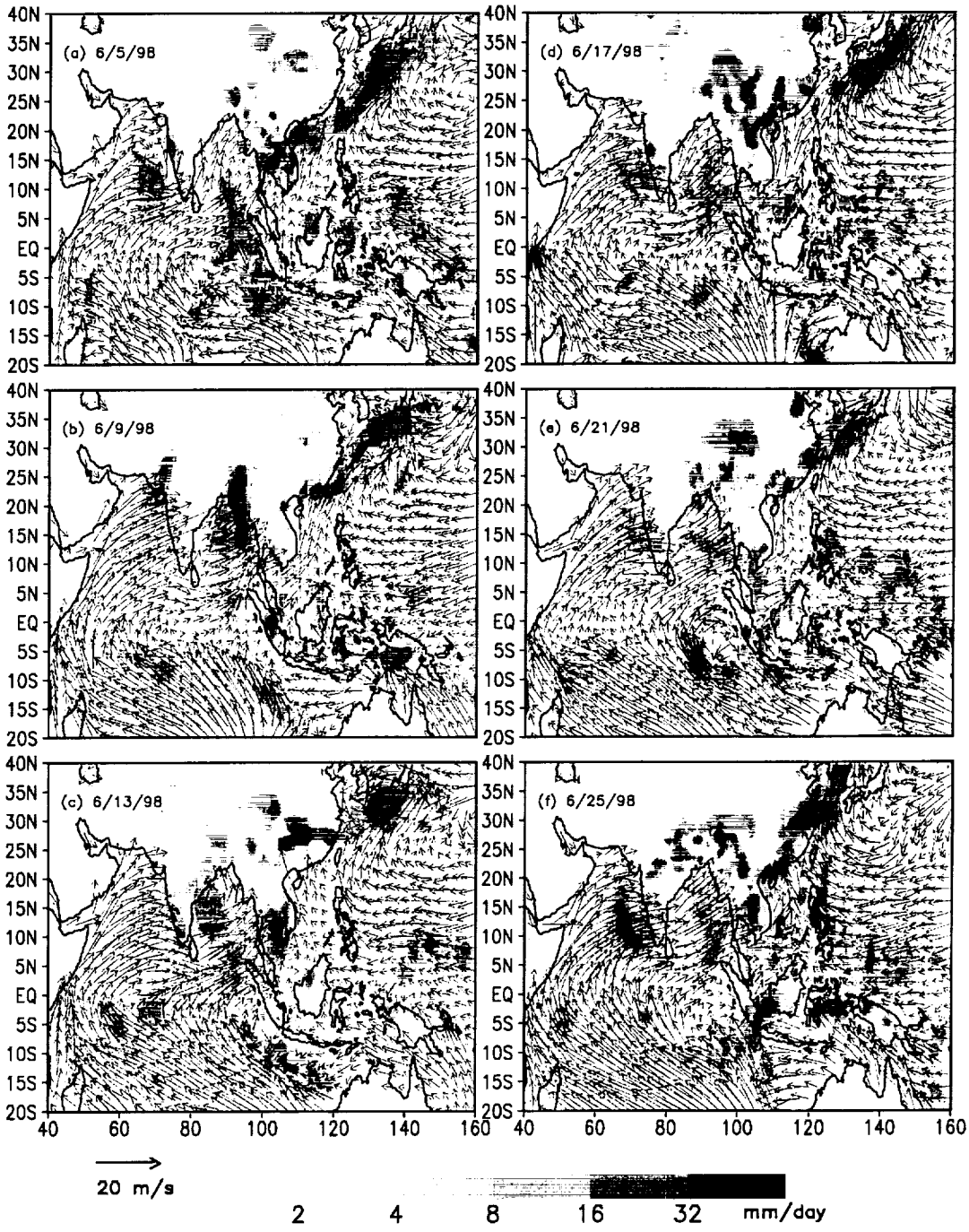
(a) 6/5/98
(b) 6/9/98
(c) 6/13/98
(d) 6/17/98
(e) 6/21/98
(f) 6/25/98
40N
35N
30N
25N
20N
15N
10N
5N
EQ
5S
10S
15S
20S
40
60
80
100
120
140
160
20 m/s
2
4
8
16
32
mm/day

Figure 3

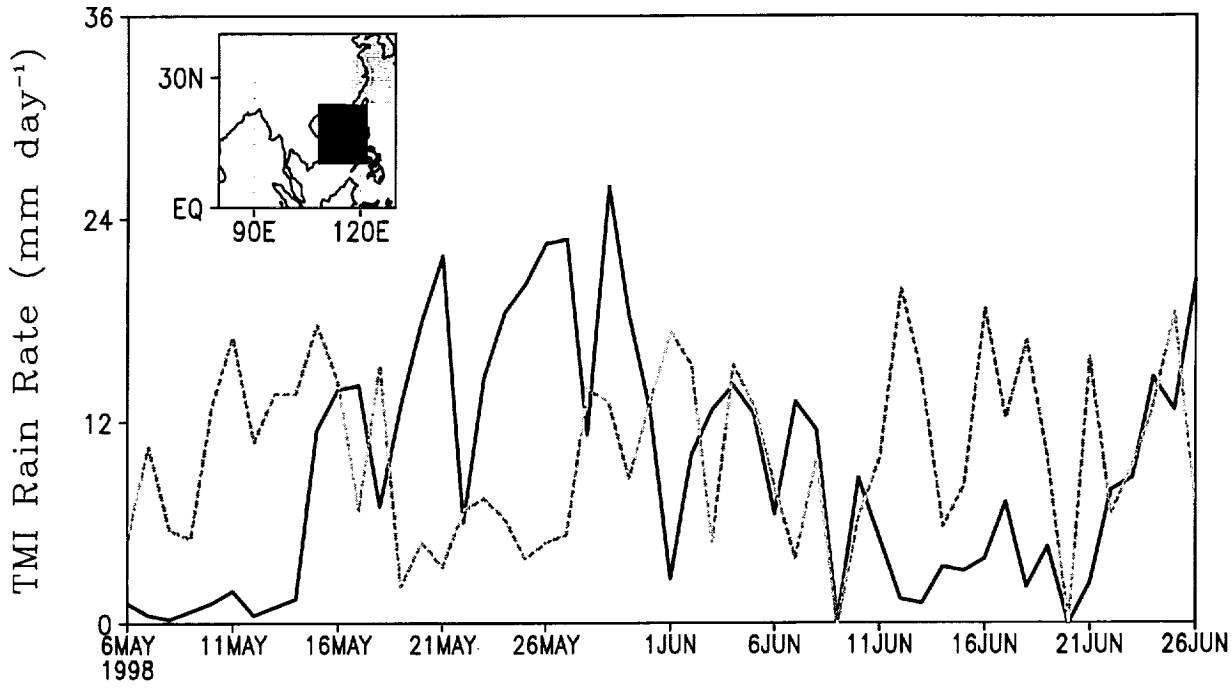
TMI Rain Rate (mm day⁻¹)
36
24
12
0
30N
EQ
90E
120E
6MAY
1998
11MAY
16MAY
21MAY
26MAY
1JUN
6JUN
11JUN
16JUN
21JUN
26JUN

Figure 4

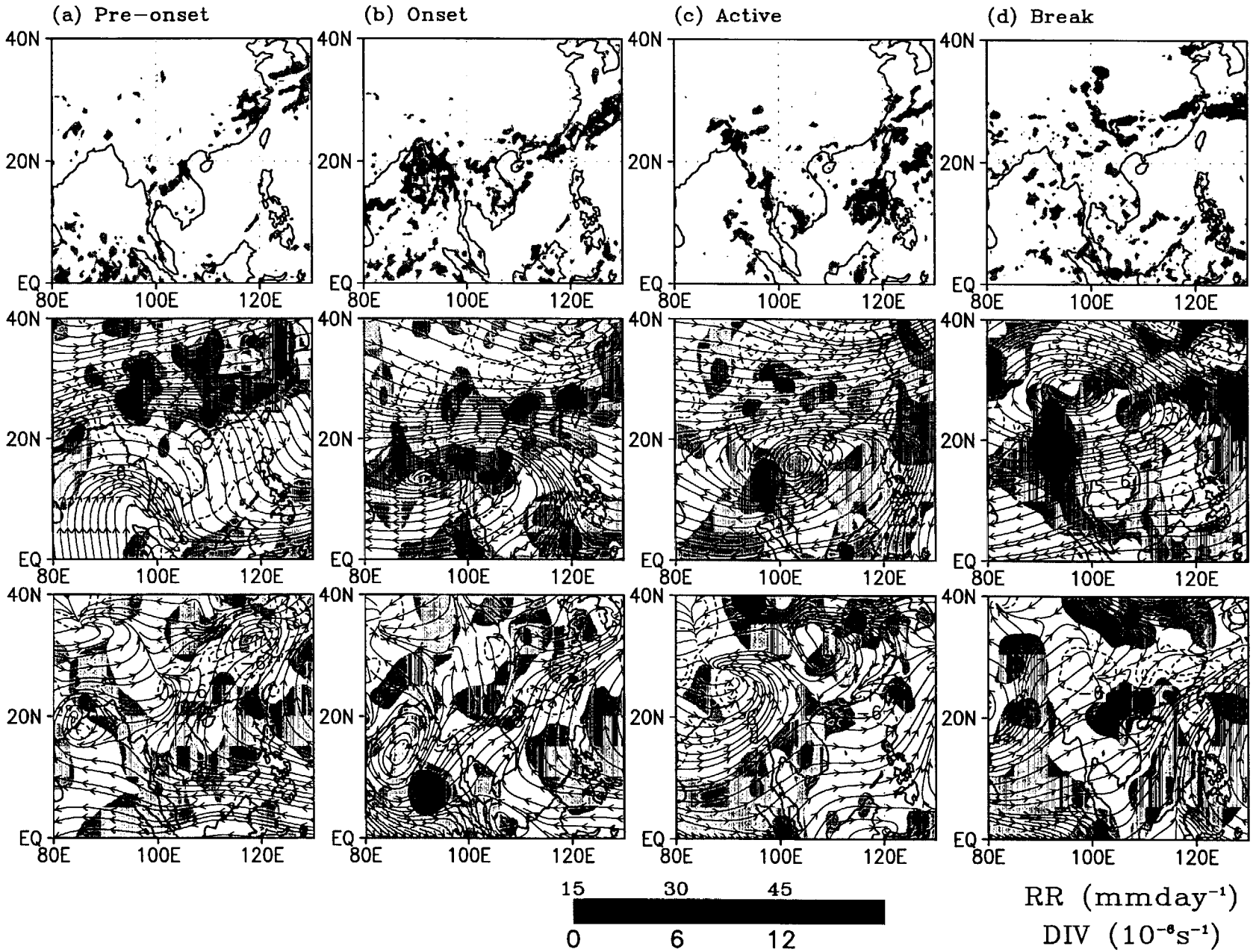
(a) Pre-onset
(b) Onset
(c) Active
(d) Break
40N
20N
EQ
80E
100E
120E
15
30
45
0
6
12
RR (mmday⁻¹)
DIV (10⁻⁶s⁻¹)

Figure 5

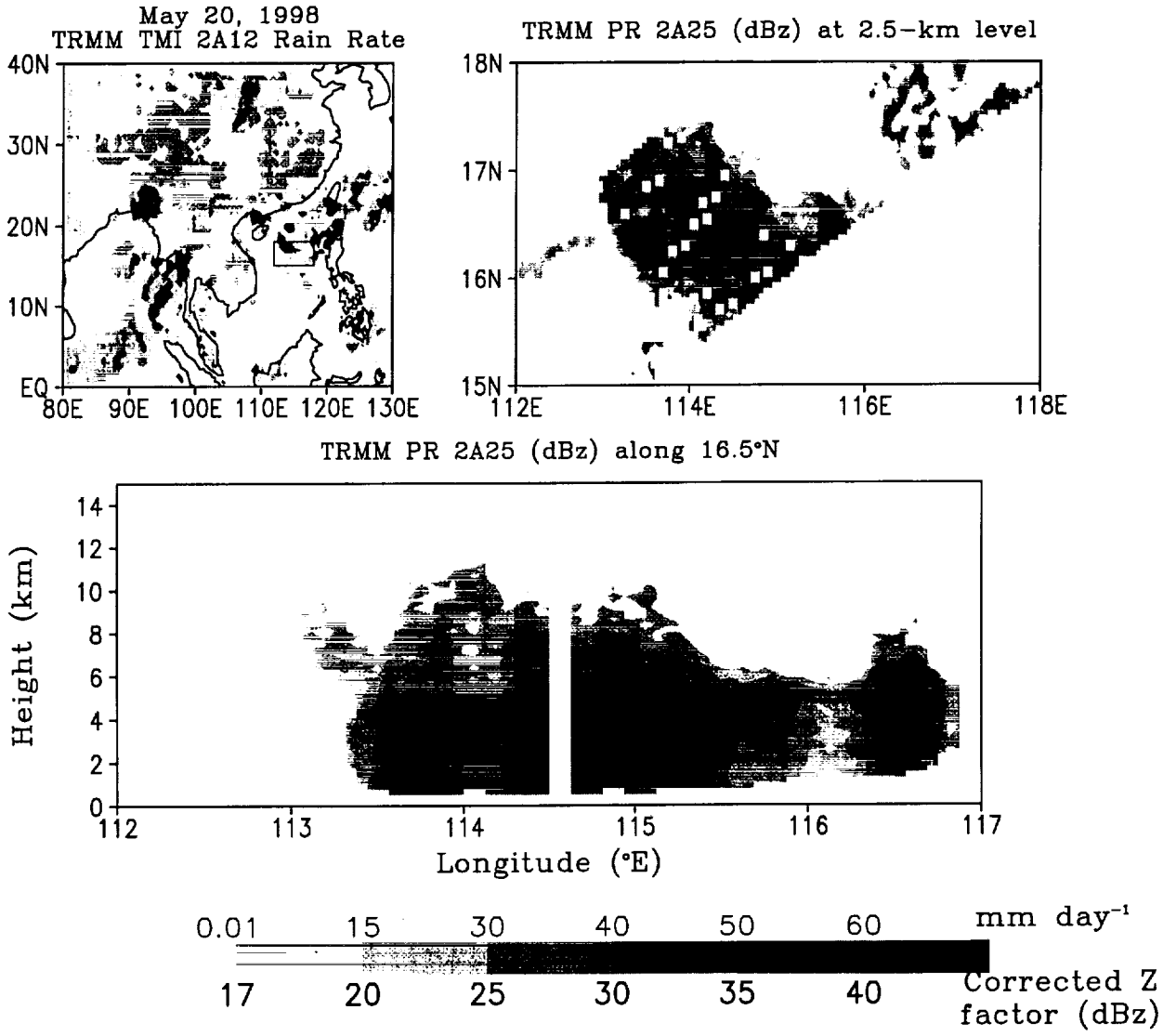
May 20, 1998
TRMM TMI 2A12 Rain Rate
40N
30N
20N
10N
EQ
80E 90E 100E 110E 120E 130E
TRMM PR 2A25 (dBz) at 2.5-km level
18N
17N
16N
15N
112E 114E 116E 118E
TRMM PR 2A25 (dBz) along 16.5°N
Height (km)
14
12
10
8
6
4
2
0
112 113 114 115 116 117
Longitude (°E)
0.01 15 30 40 50 60
mm day⁻¹
17 20 25 30 35 40
Corrected Z factor (dBz)

Figure 6

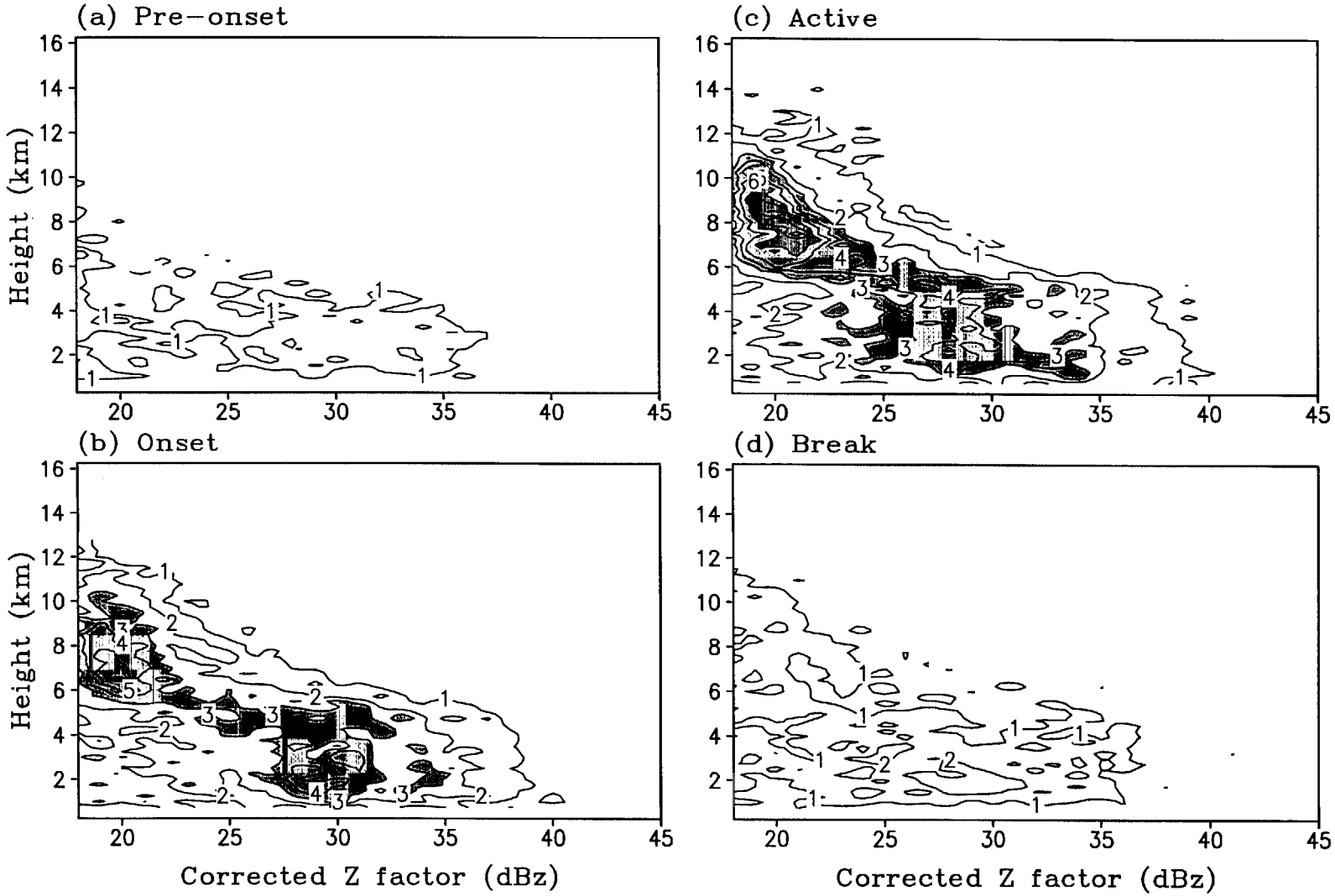
(a) Pre-onset
(c) Active
(b) Onset
(d) Break
Height (km)
Corrected Z factor (dBz)

Figure 7

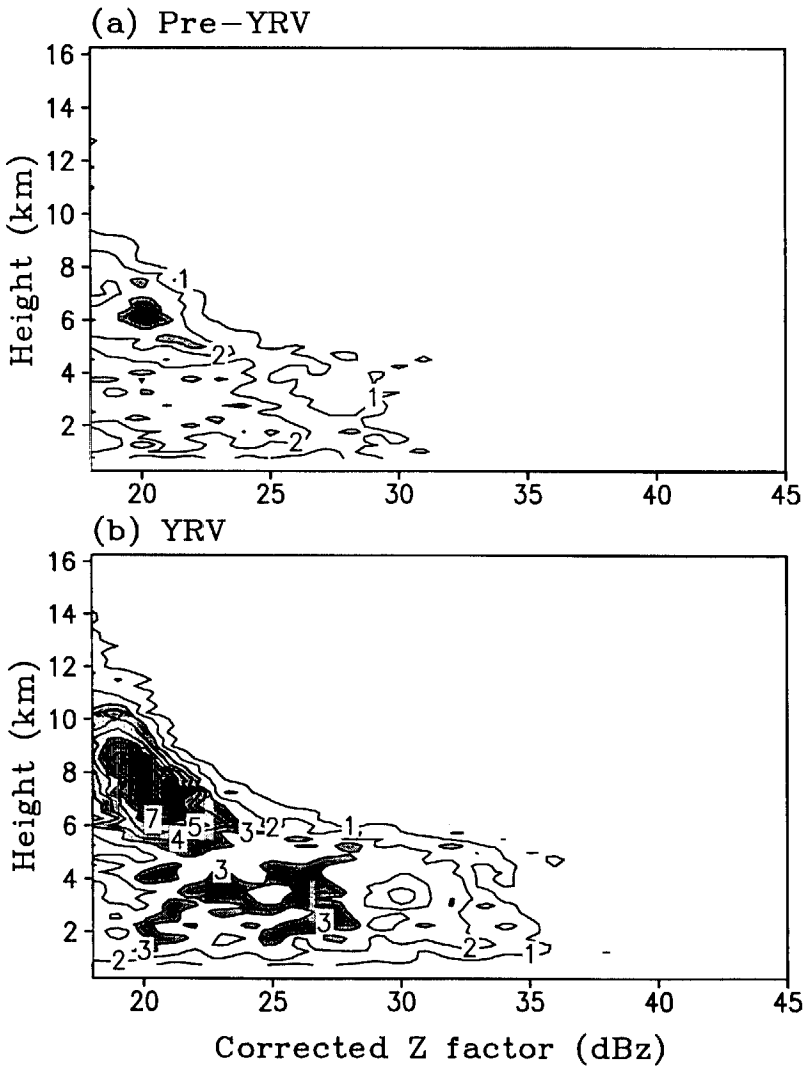
(a) Pre-YRV
(b) YRV
Height (km)
Corrected Z factor (dBz)
16
14
12
10
8
6
4
2
20
25
30
35
40
45

Figure 8

Submitted to Journal of Meteor. Soc. Of Japan

Evolution of the large scale circulation, cloud structure and regional water cycle associated with the South China Sea monsoon during May-June, 1998

K.-M. Lau[1] *and Xiaofan Li*[2]
Laboratory for Atmospheres, NASA/Goddard Space Flight Center, Greenbelt, MD

Popular Summary

The monsoon of East Asian affects the livelihood of a large segment of the world population. Understanding the physical processes needed to improve monsoon rainfall variability is critically important for agriculture, water resource management, and disaster mitigation. The South China Sea (SCS) and the eastern Indian Ocean region represents a unique region, where the Asian monsoon begins each year in mid-May, before the peak monsoon season (June-July-August) over Indian and the East Asian mainland. This region also holds the key to better monsoon rainfall prediction of large part of the East Asian continent, and the Northwestern Pacific. The South China Sea Monsoon Experiment (SCSMEX), which took place in May-June, 1998, has provided valuable field data allowing a better description of the large scale circulation and water cycle of the SCS monsoon. SCSMEX data have been most valuable in providing calibration and validation for Tropical Rainfall Mission (TRMM), which was launched in November 1997. This paper is a study of the large-scale circulation, cloud structure and water cycle of the SCS monsoon, using a combination of SCSMEX and TRMM data. We found distinct stages of the SCS monsoon development during May-June 1998, which were associated with large-scale changes in remote regions in the Indian Ocean and the western Pacific. We also found precursory signals in the Indian Ocean and the Bay of Bengal that may be important in prediction of the SCS monsoon. The water budget calculations showed that the SCS region served alternatively as a sink or source of atmospheric moisture depending on the phases of the SCS monsoon. The disastrous flooding over the Yangtze River in summer of 1998 may be due to the excessive supply of atmospheric moisture transport from the SCS into the region.

[1]Dr. William K.-M. Lau, Climate and Radiation Branch, Laboratory for Atmospheres, NASA/GSFC
[2]NOAA/NESDIS, Camp Springs, Washington DC